International Journal of Mechanical Engineering and Technology (IJMET)
Volume 9, Issue 12, December 2018, pp. 320–337, Article ID: IJMET_09_12_037
Available online at http://www.iaeme.com/ijmet/issues.asp?JType=IJMET&VType=9&IType=12
ISSN Print: 0976-6340 and ISSN Online: 0976-6359

AN ANALYTICAL FORMULA FOR DESIGNING MCKIBBEN PNEUMATIC MUSCLES

Michele Gabrio Antonelli, Pierluigi Beomonte Zobel, Walter D'Ambrogio, Francesco Durante

Department of Industrial and Information Engineering and Economics,
DIIIE, University of L'Aquila, L'Aquila, 67100. Italy

Terenziano Raparelli

Department of Mechanical and Aerospace Engineering, DIMEAS,
Politecnico of Turin, Torino, 10129. Italy

ABSTRACT

The behavior of McKibben pneumatic muscles depends on the geometrical parameters, the material properties and the functional parameters. Several formulations propose relationships among the parameters in order to predict the behavior of such type of muscles. These formulations originate from theoretical or empirical models. A formulation that includes all the parameters does not exist; the existing formulations are valid for relationships among a subset of the total amount of parameters and in specific ranges of values. In this paper, an analytical formula to predict the behavior of McKibben muscles is presented. The formula expresses the relationship among the external diameter, the thickness of the inner tube, the pressure, the contraction ratio and the developed force in a convenient range of them and for a specific material used for the inner tube. The formula was achieved by an extended campaign of simulations carried out by a previously validated finite element model of the muscle. The achieved numerical results were used to define a method, here proposed, in order to replace the finite element model with the analytical formula. The validated formula can be used as a tool to design McKibben muscles starting from technical specifications, as contraction ratio and developed force, for applications of the industrial automation and soft robotics.

Key words: Mckibben Muscles, Robotics, Finite Element Models, Pneumatics, Soft Actuators Design, Analytical Modeling.

Cite this Article: Michele Gabrio Antonelli, Pierluigi Beomonte Zobel, Walter D'Ambrogio, Francesco Durante and Terenziano Raparelli, An Analytical Formula For Designing Mckibben Pneumatic Muscles, International Journal of Mechanical Engineering and Technology, 9(12), 2018, pp. 320–337.
http://www.iaeme.com/ijmet/issues.asp?JType=IJMET&VType=9&IType=12

1. INTRODUCTION

Pneumatic artificial muscles (PAMs) are not traditional pneumatic actuators made of a closed axisymmetric elastic deformable membrane reinforced by more rigid components as kevlar, glass fiber wires, polyamide or textile braided shells, or plastic plates. Generally, when the membrane is inflated, an axial contraction follows a radial expansion and the PMA exerts a pulling force, as it happens for the straight fibers pneumatic muscles [1-3], the braided muscles [4-7], the netted muscles [8], the embedded muscles [9] and the pleated muscles [10-11]. On the contrary, a pushing force is the result of an axial membrane extension as it happens for the bellow muscles [12-17]. Like the industrial pneumatic actuators, PAMs show a high power to weight ratio; unlike the industrial pneumatic actuators, PAMs are not equipped with rigid moving components and do not require dynamic seals and lubricants. Since the high compliance of the elastic membrane, PAMs allow safety and a better acceptability in the human-machine interaction, a soft touch of fragile or delicate objects, can be adapted to various geometries, do not require rigid couplings and can recover some assembling misalignments. Nevertheless, they cannot be adopted in industrial applications where high repeatability, high precision of positioning, high speed and high durability are required. For these topics, PAMs are adopted in soft [18-21] andrehabilitation robotics [22-25], in biomechanical applications as orthotic and prosthetic devices [26-34], and they can replace smart actuators adopted in parallel robots [35,36] or electric actuators for agricultural devices [37] or for the tilting motion of 3D scanners for mobile robot navigation [38].

The braided type McKibben muscle (MKM)4-7] is the most studied and adopted. It consists of an inner elastic tube surrounded by a braided shell made of strands placed according to helical weavings. Two ends provide for the pneumatic and mechanical seals between the tube and the external shell; one of them, for the air inlet/outlet. When the inner tube is inflated, the MKM radially bulges and shortens, due to the not extensible strands of the shell that act like a pantograph. The relationship “Force-Pressure-Contraction” of the MKM depends on the following parameters: the geometry (diameter and thickness of the tube at rest, angle of the strands at rest), the material of the inner tube, the operating air pressure value and the external tensile force applied to the muscle. Several formulations among these parameters were achieved by theoretical models. Some of them were based on the energy conservation: Shulte [4] proposed an analytical formulation of the MKM modelled as an ideal cylinder whose behavior depends on the elastic properties of the material of the tube and on the energy dissipation due to the internal friction; in a first study [6] Chou and Hannaford added the effect of the tube thickness and extended the application of the formulation of Shulte; then, they achieved an analytical formulation [39] taking into account the hyper-elasticity of the material of the tube by the Mooney-Rivlin formulation. Some models were developed to take into account the real shape of the tube near the ends during the shortening phase [7,39] and the effect of the friction among the wires of the braided shell [7,41,42]. Nevertheless, the practical application of these models is limited because of their complexity, some parameters are difficult to be measured or evaluated and some formulations are valid in particular ranges of geometrical parameters. Probably, for this reason PAMs have been mainly studied in research activities and, typically, self-made by researchers. Only a few number of PAMs are available on the market: the MAS and DMSP of Festo AG and the Shadow Air Muscles of Shadow Robot Company, as for the knowledge of the authors. The relationship between the applied load and the internal pressure can be predicted by a theoretical model [43] that takes into account the geometry of the braided shell.

More recently, some researchers [44] proposed an analytical formula, achieved by experimental prototypes, capable to calculate the relationship among the developed force at a given pressure, contraction and for a known geometry. Moreover, they defined an

experimental method to achieve the value of certain correcting factors to perform the design of several size of MKMs.

This paper proposes an analytical formula of the relationship "Force-Pressure-Contraction" in a MKM, validated in a convenient range of arbitrary values of the thickness, the diameter and the pressure, and for a given material of the inner tube. The formula was achieved by an extensive campaign of simulations carried out by a non-linear finite element model of a MKM, experimentally validated in a previous activity as described in [45]. The formula predicts the behavior of MKMs made of the same material and, hence, facilitates the design of them according to the proper specifications depending on different applications.

2. BACKGROUND

2.1 The McKibben pneumatic muscle

The working principle of the MKM is shown in Figure 1: when the air pressure P is applied inside the inner tube, the muscle radially bulges; due to the not extensible strands of the braided shell that act like a pantograph, the expansion force in the radial direction is converted into a force F in the axial direction that provides for the contraction of the muscle. One terminal end is equipped with a pneumatic fitting for the air inlet/outlet.

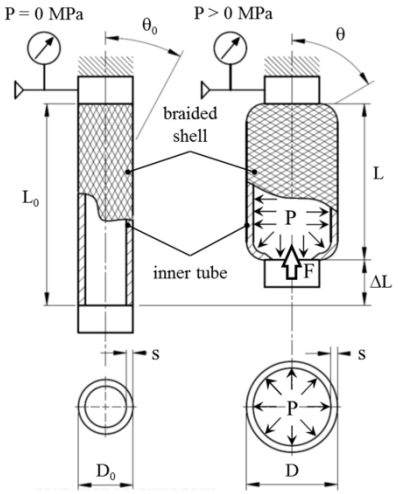

Figure 1 The working principle of the McKibben pneumatic muscle: at rest and when compressed air is inflated at a pressure P

The theoretical formulation of the relationship "Force (F)-Pressure(P)-Contraction($\Delta L/L_0$)", based on the values of D_0 and θ_0 and widely recognized by several researchers [46-49] is:

$$F = (\pi D_0^2 P/4 \cdot sin^2\theta_0)[3(1-\Delta L/L_0)^2 cos^2\theta_0 - 1] \quad (1.1)$$

or equivalently [4]:

$$F = (\pi D_0^2 P/4)[3cos^2\theta - 1] \quad (1.2)$$

considering the geometrical relationships of a pantograph system, applied to one strand:

$$L_0/cos\theta_0 = L/cos\theta, \quad D_0/sin\theta_0 = D/sin\theta \quad (2)$$

The formulations (1) do not include the effect of the thickness of the inner tube: it is assumed that a perfect cylinder with a zero wall thickness simulates the actuator and that *s* has a null value. Nevertheless, an amount of the pressure energy must be converted into deformation energy of the tube, dependent on the real volume of it and, hence, on the thickness. Due to the same assumption, they do not consider the effects of the rounding of the

terminal ends. Finally, they suppose that the force starts to be applied at an initial contraction corresponding to a zero value of the pressure P. Nevertheless, in some applications, it could happen that the MKM freely contracts until a fixed rate, corresponding to a P' value, without exerting force; then, it keeps on the contraction, over P', and develops an incremental force. In this case, it is difficult to achieve P' without an experimental activity. These topics limit the application of (1) for the design of MKMs.

Recently, Belforte et al.[44] proposed a novel formulation:

$$F = P \cdot [(L_0 - \Delta L)/2] \cdot \left[\sqrt{(b^2 - (L_0 - \Delta L)^2)/\pi}\right]\left(b^2 - {L_0}^2 - \Delta L^2 + 2L_0\Delta L\right)^{-\frac{1}{2}} - -P(\pi/4)\left[\sqrt{(b^2 - (L_0 - \Delta L)^2)/\pi}\right] \quad (3)$$

where b, the length of every strand that forms the braided shell, includes the effects of the rounding of the terminal ends. The formulation (3) was validated by experimental tests carried out by five MKM prototypes. Nevertheless, it does not include the effect of the thickness and, directly, of the diameter of the inner tube: experimental prototypes had the same thickness and the same diameter.

2.2. The validated finite element model

In order to have a suitable design tool of MKMs, capable to apriori describe their behavior and taking into account the geometry at rest, the thickness and the rounding of the terminal, a 3D non-linear parametric finite element (FE) model, hereinafter called model, was developed [45]. L_0, D_0, θ_0, and s are the geometrical input parameters. The model can simulate two types of tests in quasi-static conditions: isometric (the force F developed by the muscle is computed as function of the pressure P, at a fixed contraction ratio $\Delta L/L_0$) and isotonic (the contraction ratio $\Delta L/L_0$ of the muscle is computed as function of the pressure P, at a constant tensile force F applied to one terminal end) tests. Additional input parameters are: the maximum operating pressure P; moreover, the necessary shortening ΔL, to obtain the wanted contraction ratio, or the tensile force F for the isometric or the isotonic tests, respectively. The output parameters are computed in the pressure range (0.00 – P) for every incremental step of the pressure equal to 0.01 MPa. Frictional forces between the shell and the tube are neglected: this choice was experimentally validated [45]. Hysteretic behavior and the time dependent behavior were neglected. Due to the double symmetry of the muscle, axisymmetric geometry and as regards the plane perpendicular to the axis of the muscle, the model simulates one eighth of the real geometry.

Brick elements are adopted for the inner tube and for the terminal end; truss ones for the braided shell. The high deformable elastic material of the inner tube is simulated as hyper-elastic by two coefficients of the first-order of the Mooney-Rivlin formulation; the material of the shell and of the terminal end are simulated as isotropic. Symmetric constrains are applied in correspondence of the symmetry planes. Pressure P is perpendicularly applied on the internal surface of the inner elements of the tube, from zero to the input value. The same procedure is adopted for the force F: due to the symmetry, a quarter of the total force value is applied to the center of the upper surface of the terminal end. A non-linear analysis, based on the Newton-Raphson method, is implemented. The construction of the model (nodes, elements, material types, constraints, loads and analysis parameters) is given to the FE software as a script file generated by an algorithm running on a commercial computing language. Some pictures of the model, with loads and constraints application, are shown in Figure 2.

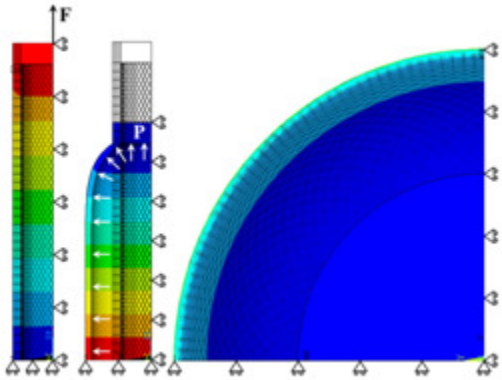

Figure 2 The FE model of the MKM: force F and pressure P, symmetry constraints and the behavior of the rounding of the terminal end are shown

For the validation of the model, an experimental activity was carried out by a MKM prototype, shown in Figure 3, at different contraction ratios, with the following peculiarities: L_0=285 mm; D_0=30 mm; s=3 mm; inner tube in Dow Corning SILASTIC S silicone rubber for moulds; commercial braided shell tube in Polyamide 66 with θ_0=28°, available for several sizes of diameter; terminal ends in aluminum. Finally, in order to assure pneumatic and mechanical seals, the prototype is equipped with terminal ends whose design was proposed as novel solution for the assembly of a MKM.

The model was validated by the comparison among numerical and experimental results of tests of the same type: isotonic tests at three force values, 20, 80 and 150 N; isometric tests at three contraction ratios, 0%, 45% and 90% of the maximum contraction. The qualitative good fitting of the numerical and experimental curves outlined the validation of the model. Hence, correlation and linear regression analyses, among numerical and experimental data, gave quantitative good results: coefficient R^2 is equal to 0.99 for each test. These achievements validated the model. Then, the model was adopted to design MKMs, made of the same silicone rubber. Nevertheless, the availability of the FE software was required. Hence, the achievement of the proper set of parameters, for a specific application, required several attempts with a consequent high amount of simulation time.

For these reasons, the model was thought to be used as a tool for an extensive campaign of simulations in order to collect data in convenient ranges of diameter, thickness and pressure; hence, the data processing to achieve the formula of the relationship "Force-Pressure-Contraction". On the one hand, the formula could replace the FE model; on the other one, the formula could fill the lack of a formulation that takes into account the effect of the thickness and the combined effect of diameter, thickness and pressure values.

Figure 3 The experimental prototype of the McKibben pneumatic muscle at different contraction ratios

3. MATERIALS AND METHODS

3.1. The effect of the thickness: preliminary considerations

The effect of D_0 on the behavior of a MKM is clearly explained by (1): an increase of the diameter causes an increase of the developed force, according to a quadratic law. On the contrary, the effect of s is neglected. As previously mentioned, this effect must necessarily be considered. To demonstrate this assumption, the FE model was adopted. A first set of simulations was carried out with a model simulating the experimental prototype of the MKM, with the exception of the thickness: three isometric tests at shortenings ΔL=0 mm, ΔL=20 mm and ΔL=40 mm, for five thickness values (1, 2, 3, 4 and 5 mm) were simulated. Simulations for thickness values under 1 mm produced convergence errors; moreover, tubes with thickness of such values are complex to be realized by moulding and are not convenient for a real application. Numerical results were compared to the Force-Pressure curves obtained by (1), at the same contraction ratios and for D_0=24 mm (equivalent to the internal diameter of the experimental MKM). For the same thickness values, a second set of three simulated isotonic tests was carried out at F=20 N, F=80 N and F=150 N. Numerical results were compared to the Shortening-Pressure curves obtained by the rearrangement of (1), as follows:

$$\Delta L = L_0 \left\{1 - \sqrt{(1/(3 \cdot cos^2\theta_0)\{1 + [4sin^2\theta_0/(\pi D_0^2)] \cdot (F/P)\}}\right\} \quad (4)$$

where not congruent negative values of ΔL, resulting from the calculus, were neglected and the pressure corresponding to the zero value of ΔL was set as zero pressure. Results are shown in Figure 4.

In isometric tests, regardless of the thickness, an increase of the contraction level causes a decrease of the slopes of the Force-Pressure curves. Taking into account the increase of the thickness, it causes a decrease of the slope of the Force-Pressure curve, corresponding to a decrease of the developed force, that can reach about 300 N, at the same pressure and for the same ΔL.

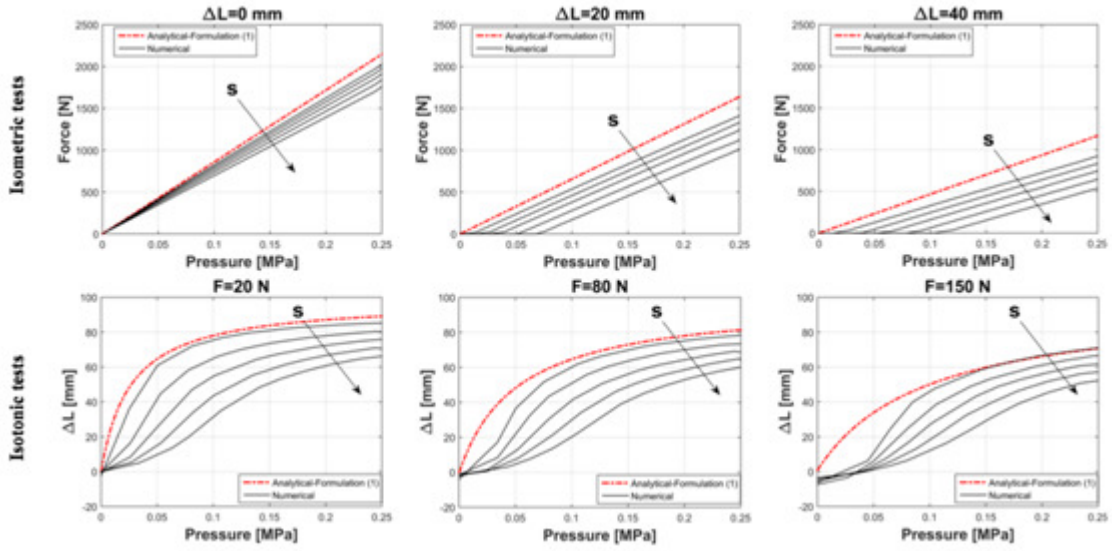

Figure 4 The effect of the thickness (s=1, 2, 3, 4 and 5 mm) of the tube in isometric and isotonic tests

Moreover, for the same ΔL and with the exception of ΔL=0, the increase of the thickness requires higher pressure to reach the settled contraction level, from which the MKM starts to develop the force. The maximum pressure gap can reach about 0.07 MPa. The analytical curves show slopes higher than the numerical ones, due to the hypothesis of the zero wall

thickness. Finally, (1) does not allow to achieve the pressure value corresponding to the achievement of the settled contraction rate; on the contrary, the FE model provides for it. In isotonic tests, the thickness s has the same effect of the external applied force: its increase causes a decrease of the contraction level and a reduction of the slope of the Displacement-Pressure curves. The analytical curves show higher shortenings than the numerical ones. In isometric and isotonic tests, respectively, the slopes and the behavior of s=1 mm numerical curves, the nearest to the null thickness ones, are quite similar to the analytical ones: this result is a further indication of the goodness of the model to simulate the effect of the thickness on the behavior of a MKM.

3.2. Force-Contraction curves

Force-Contraction curves, as function of the maximum operating pressure, are the operative graphs for the proper choice of a MKM, according to the specific application. These curves give information about the force developed by a MKM, with a known geometry in terms of D_0 and s, at a given contraction ratio and pressure.

They are obtained by processing the results of the isometric tests. With reference to the isometric curves of Figures 4, for a given thickness, it is possible to calculate the force developed by the muscle at a given contraction level and at the same pressure by the intersection of vertical straight lines, one for each desired value of pressure, with the Force-Pressure curve. The detected intersection points, in a Force-Contraction diagram, implement the isobaric Force-Contraction curves, as shown in Figure 5. As in isometric tests, the increase of pressure, at the same contraction level, causes the increase of the developed force; on the contrary, the increase of the contraction level, at the same pressure, causes a decrease of the force.

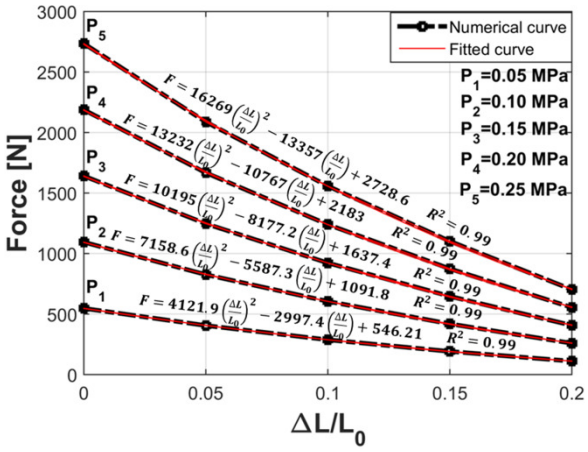

Figure 5 Example of Force-Contraction curves at a given thickness and diameter

Moreover, it is interesting to notice that all the numerical curves can be accurately described (R^2 equal to 0.99) by quadratic polynomial fitting curves, whose formulation can be expressed as:

$$F = a \cdot (\Delta L/L_0)^2 + b \cdot (\Delta L/L_0) + c \quad (5)$$

where the values of the coefficients a, b and c depend on the values of the pressure P, the thickness s and the diameter D_0. Hence,

$$a = A(P, s, D_0) \quad (6.1)$$

$$b = B(P, s, D_0) \quad (6.2)$$

$$c = C(P, s, D_0) \tag{6.3}$$

This assumption is demonstrated in Figure 6. Isobaric surfaces were obtained by processing the results of several simulations, later described. In particular, the increase of the thickness confirms, at a given diameter and pressure, a decrease of the developed force; in accordance with (1), the increase of the diameter causes, at a given thickness and pressure, an increase of the developed force. The effect of the initial length L_0 on the behaviour of a MKM is included in the definition of the imposed contraction ratio $\Delta L/L_0$. On the basis of (5, 6), the formula "*Force-Pressure-Contraction*", that includes all the points belonging to surfaces similar to those ones shown in Figure 6, can be expressed as:

$$F = A \cdot (\Delta L/L_0)^2 + B \cdot (\Delta L/L_0) + C \tag{7}$$

It is necessary to find the formulations of A, B and C as function of P, s and D_0. Then $F=F(P, s, D_0, \Delta L/L_0)$ can be achieved.

3.3. The proposed method

An extensive campaign of simulations was carried out by numerical models built on the basis of the following parameters:

- 4 values of D_0: 30, 40, 45 and 50 mm, called D_1, D_2, D_3, D_4, respectively;
- 5 values of s: 1, 2, 3, 4 and 5 mm, called s_1, s_2, s_3, s_4 and s_5, respectively;
- 5 ratios of $\Delta L/L_0$: 0.00, 0.05, 0.10, 0.15 and 0.20;
- maximum operative pressure equal to 0.25 MPa; the incremental step of the pressure was set equal to 0.01 MPa.

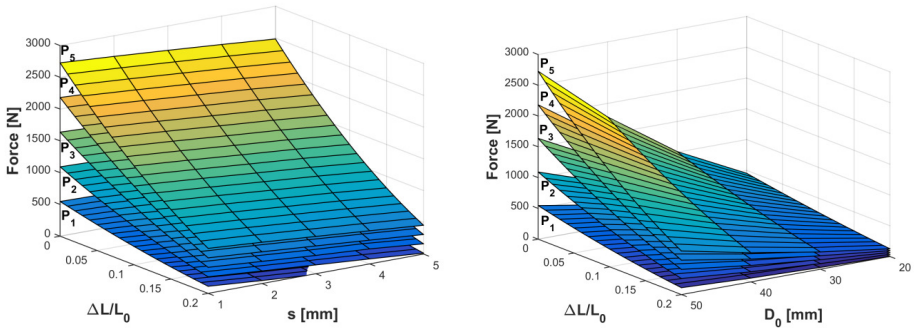

Figure 6 Force-Contraction curves as function of the pressure P and: a) s, at a given D_0; b) D_0, at a given s

Moreover, θ_0 was fixed equal to 28° for all the models, due to the commercial availability of several sizes of braided shell with such value.

For each value of D_0, 5 models were built with different values of s; for each model, 5 isometric tests were simulated at the different contraction ratios. An overall amount of 100 simulations was carried out. For each couple (D,s), 26 Force-Contraction curves were achieved, for all the pressure steps, in the range 0.00-0.25 MPa, for an overall amount of 520 curves. Due to the proximity of the curves inside a range equal to 0.05 MPa, among the 26 curves, only 5 curves, corresponding to the following five levels of pressure, were considered: 0.05, 0.10, 0.15, 0.20 and 0.25 MPa called P_1, P_2, P_3, P_4 and P_5, respectively. For couples (D,s) with diameters lower than 35 mm and thickness higher than 3 mm, the curves at 0.05 MPa were considered only in the range 0.00-0.05 of $\Delta L/L_0$. Models with values of D_0 lower than 30 mm were neglected for incompleteness of significant curves: for thickness lower than 3 mm, the Force-Contraction curves are described by only two points so that the method cannot be applied. The whole set of processed curves satisfied the formulation (5).

In order to express the coefficients A, B and C as function of the geometrical parameters D_0 and s and of the functional parameter P, the following detailed method was defined and implemented. The first part of the method was focused to achieve the formulations of the coefficients A, B and C as function of s and P; then, the method was focused to achieve the final formula including the dependence on D_0.

3.3.1. Dependence on s and P, at a given D0

1. for a given value of D_0, the numerical Force-Contraction curves for each value of s were fitted by quadratic polynomial curves;

2. for a given value of s, for each pressure level, five values of the coefficients a, b, c of the polynomial curves were collected:

$a_{\bar{s},P_i}(\bar{\mathbf{D}})$, $b_{\bar{s},P_i}(\bar{\mathbf{D}})$ and, $c_{\bar{s},P_i}(\bar{\mathbf{D}})$i=1, 2, 3, 4, 5

With reference to Figure 4, an example of the collected coefficients is reported in Table 1. According to the International Systems of Units, a, b and c are measured in [N].

Table 1 Coefficients at a given D_0 and s

P [MPa]	a [N]	b [N]	c [N]
0.05	4121.9	-2997.4	546.21
0.10	7158.6	-5587.3	1091.8
0.15	10195	-8177.2	1637.4
0.20	13232	-10767	2183
0.25	16269	-13357	2728.6

3. in order to find the relationship between the coefficients and the pressure P, given

$\mathbf{P} = (P_1, P_2, P_3, P_4, P_5)$, $a_{\bar{s}_j,\mathbf{P}}(\bar{\mathbf{D}})$, $b_{\bar{s}_j,\mathbf{P}}(\bar{\mathbf{D}})$ and $c_{\bar{s}_j,\mathbf{P}}(\bar{\mathbf{D}})$j=1, 2, 3, 4, 5

were plotted. All the models showed the same behavior: the coefficients linearly change with the pressure. As regards a: for values of D_0 in the range 35-50 mm, an increase of the pressure causes an increase of a, at the same thickness (same result can be achieved by Table 1) and an increase of s causes an increase of a, at the same pressure; for values of D_0 under 35 mm, a shows an opposite behavior. As regards b, an increase of the pressure causes a decrease of b, at the same thickness (same result can be achieved by Table 1) and an increase of s causes a decrease of b, at the same pressure. As regards c, an increase of the pressure causes an increase of c, at the same thickness (same result can be achieved by Table 1) and an increase of s causes a decrease of c, at the same pressure.

Figure 7 shows an example of these behaviors.

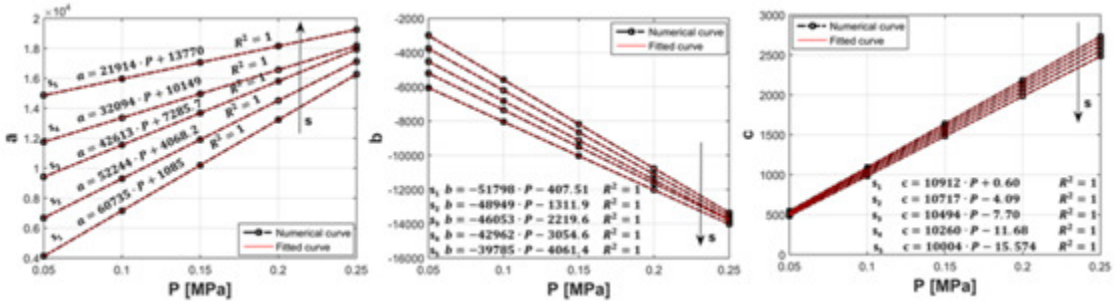

Figure 7 Behaviors of the coefficient a, b and c as function of the pressure P and the thickness s, at a given D_0

4. the previous step demonstrates that a, b and c, as regards the pressure, can be written as:

$$a_{\bar{s}_j,\boldsymbol{P}}(\bar{\mathbf{D}}) = m_a(\bar{s}_j)\cdot P + q_a(\bar{s}_j) \quad (8.1)$$

$$b_{\bar{s}_j,\boldsymbol{P}}(\bar{\mathbf{D}}) = m_b(\bar{s}_j)\cdot P + q_b(\bar{s}_j) \quad (8.2)$$

$$c_{\bar{s}_j,\boldsymbol{P}}(\bar{\mathbf{D}}) = m_c(\bar{s}_j)\cdot P + q_c(\bar{s}_j) \quad (8.3)$$

In order to explicit the dependence on s and P, the slopes $\mathbf{m}(\bar{s}_j)$, measured in [mm^2], and the y-intercepts $\boldsymbol{q}(\bar{s}_j)$, measured in [N], were plotted as function of s. The obtained curves can be accurately described by quadratic polynomial fitting curves. Figure 8 shows an example of the curves and their fittings.

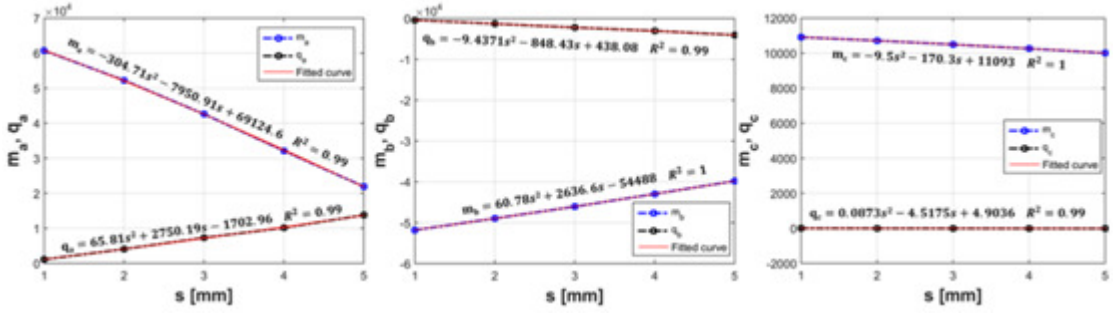

Figure 8 Behaviors of the coefficient of the linear regression of a, b and c as function of thickness s, at a given D_0

5. the resulting formulations of the coefficients a, b and c, depending on s and P, can be written as:

$$a_{\bar{\mathbf{D}}} = \left(a_{1,\bar{\mathbf{D}}}\cdot s^2 + a_{2,\bar{\mathbf{D}}}\cdot s + a_{3,\bar{\mathbf{D}}}\right)\cdot P + \left(a_{4,\bar{\mathbf{D}}}\cdot s^2 + a_{5,\bar{\mathbf{D}}}\cdot s + a_{6,\bar{\mathbf{D}}}\right) \quad (9.1)$$

$$b_{\bar{\mathbf{D}}} = \left(b_{1,\bar{\mathbf{D}}}\cdot s^2 + b_{2,\bar{\mathbf{D}}}\cdot s + b_{3,\bar{\mathbf{D}}}\right)\cdot P + \left(b_{4,\bar{\mathbf{D}}}\cdot s^2 + b_{5,\bar{\mathbf{D}}}\cdot s + b_{6,\bar{\mathbf{D}}}\right) \quad (9.2)$$

$$c_{\bar{\mathbf{D}}} = \left(c_{1,\bar{\mathbf{D}}}\cdot s^2 + c_{2,\bar{\mathbf{D}}}\cdot s + c_{3,\bar{\mathbf{D}}}\right)\cdot P + \left(c_{4,\bar{\mathbf{D}}}\cdot s^2 + c_{5,\bar{\mathbf{D}}}\cdot s + c_{6,\bar{\mathbf{D}}}\right) \quad (9.3)$$

Hence, the first approximation of the formulation "Force-Pressure-Contraction", as function of s and P, can be expressed as:

$$F = \{[A_1(D_0)\cdot s^2 + A_2(D_0)\cdot s + A_3(D_0)]P + [A_4(D_0)\cdot s^2 + A_5(D_0)\cdot s + A_6(D_0)]\}\cdot\left(\frac{\Delta L}{L_0}\right)^2$$

$$+\{[B_1(D_0)\cdot s^2 + B_2(D_0)\cdot s + B_3(D_0)]P + [B_4(D_0)\cdot s^2 + B_5(D_0)\cdot s + B_6(D_0)]\}\cdot\left(\frac{\Delta L}{L_0}\right)$$

$$+\{[C_1(D_0)\cdot s^2 + C_2(D_0)\cdot s + C_3(D_0)]P + [C_4(D_0)\cdot s^2 + C_5(D_0)\cdot s + C_6(D_0)]\} \quad (10)$$

where, given D = (D_1, D_2, D_3, D_4),

$A_k(D_0)$is the polynomial expression that fits $a_k(\mathbf{D})$ *k=1, 2, 3, 4, 5, 6*

$B_k(D_0)$is the polynomial expression that fits $b_k(\mathbf{D})$ *k=1, 2, 3, 4, 5, 6*

$C_k(D_0)$ is the polynomial expression that fits$c_k(\mathbf{D})$ *k=1, 2, 3, 4, 5, 6*

3.3.2. Dependence on D

The second part of the method was focused to explicit $a_k(\mathbf{D})$, $b_k(\mathbf{D})$ and $c_k(\mathbf{D})$as function of D_0.

6. $a_k(\mathbf{D})$, $b_k(\mathbf{D})$ and $c_k(\mathbf{D})$were plotted, as shown in Figures 9, 10 and 11, respectively.

7. the best fitting polynomial curves were considered to describe the dependence of $a_k(\mathbf{D})$,$b_k(\mathbf{D})$and $c_k(\mathbf{D})$on D_0.A and B coefficients can be accurately described by quadratic polynomial fitting curves, with the exception of coefficients C, whose relationship between $c_k(\mathbf{D})$and D_0 can be described, not too much accurately, by linear fitting curves.

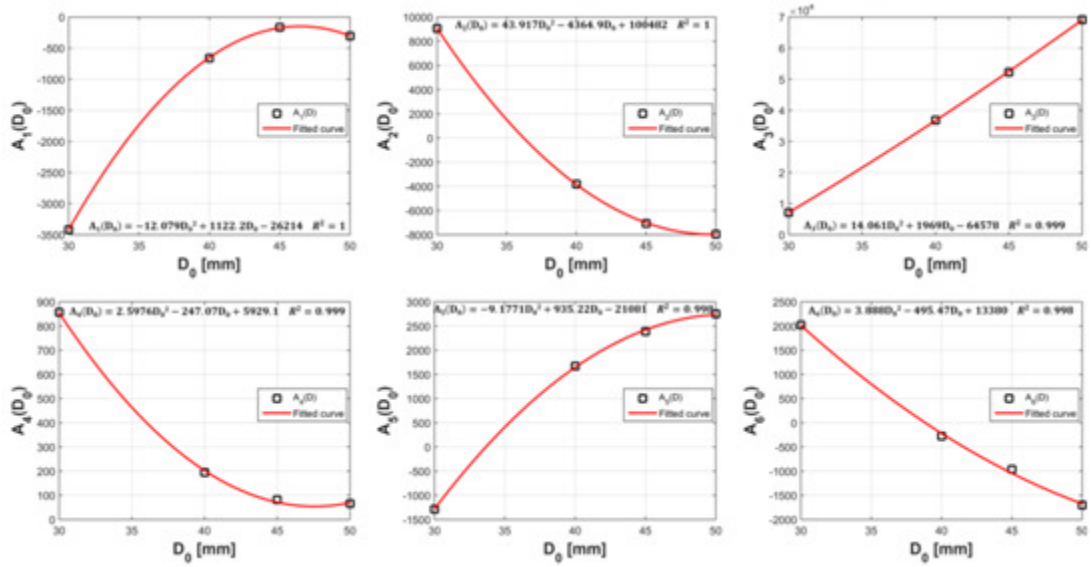

Figure 9 Behaviors of $a_k(\mathbf{D})$

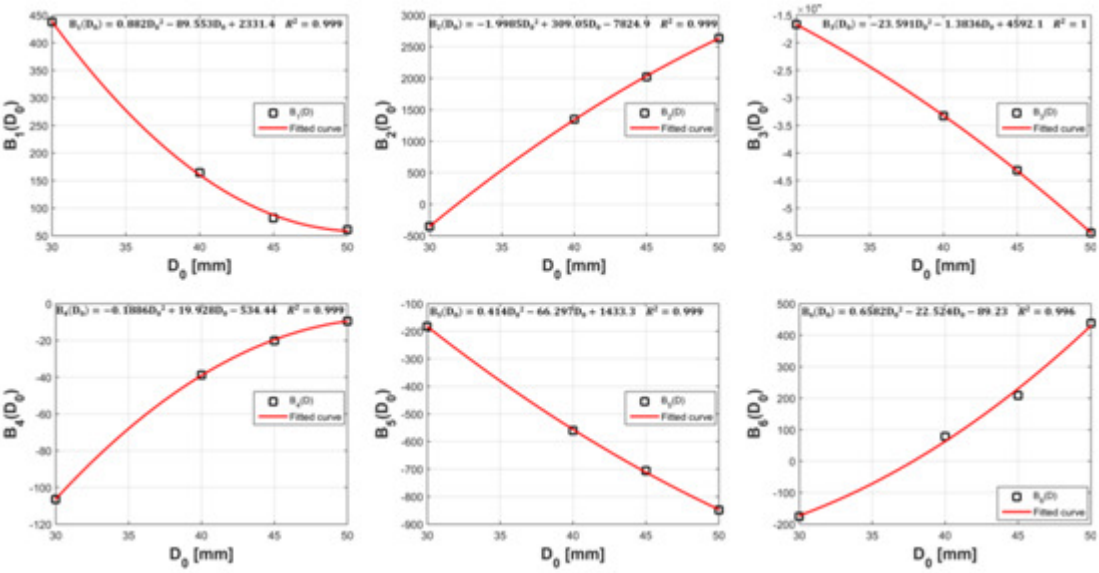

Figure 10 Behaviors of $b_k(\mathbf{D})$

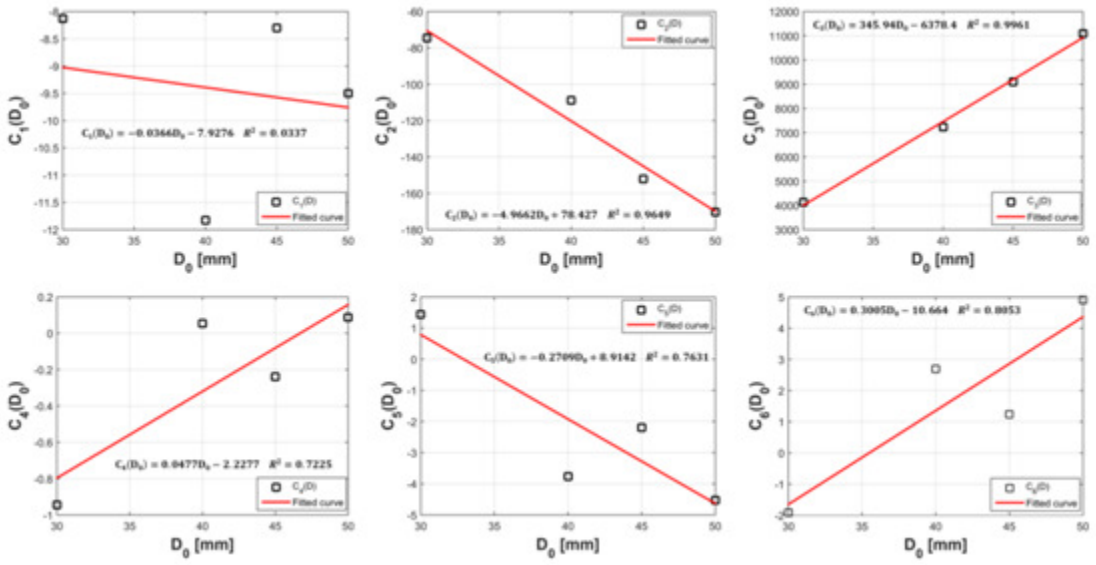

Figure 11 Behaviors of $c_k(\mathbf{D})$

3.3.3. Final formulation

On the basis of the previous results, the final formulation "*Force-Pressure-Contraction*" can be expressed as follows:

$$\mathbf{F} = \left\{ \begin{bmatrix} (A_{11}\cdot \boldsymbol{D_0^2} + A_{12}\cdot \boldsymbol{D_0} + A_{13})\boldsymbol{s^2} + \begin{matrix}(A_{21}\cdot \boldsymbol{D_0^2} + A_{22}\cdot \boldsymbol{D_0} + A_{23})\boldsymbol{s} + \\ +(A_{31}\cdot \boldsymbol{D_0^2} + A_{32}\cdot \boldsymbol{D_0} + A_{33})\end{matrix} \end{bmatrix} \boldsymbol{P} \right\} \cdot \left(\frac{\Delta L}{L_0}\right)^2 +$$

$$+ \left\{ \begin{bmatrix} (B_{11}\cdot \boldsymbol{D_0^2} + B_{12}\cdot \boldsymbol{D_0} + B_{13})\boldsymbol{s^2} + \begin{matrix}(B_{21}\cdot \boldsymbol{D_0^2} + B_{22}\cdot \boldsymbol{D_0} + B_{23})\boldsymbol{s} + \\ (B_{31}\cdot \boldsymbol{D_0^2} + B_{32}\cdot \boldsymbol{D_0} + B_{33})\end{matrix} \end{bmatrix} \boldsymbol{P} \right\} \cdot \left(\frac{\Delta L}{L_0}\right) +$$

$$+ \left\{ \begin{bmatrix} (C_{11}\cdot \boldsymbol{D_0^2} + C_{12}\cdot \boldsymbol{D_0} + C_{13})\boldsymbol{s^2} + \begin{matrix}(C_{21}\cdot \boldsymbol{D_0^2} + C_{22}\cdot \boldsymbol{D_0} + C_{23})\boldsymbol{s} + \\ (C_{31}\cdot \boldsymbol{D_0^2} + C_{32}\cdot \boldsymbol{D_0} + C_{33})\end{matrix} \end{bmatrix} \boldsymbol{P} \right\} \qquad (11)$$

$$+ \begin{bmatrix} C_{41}\cdot \boldsymbol{D_0} + C_{42})\boldsymbol{s^2} + (C_{51}\cdot \boldsymbol{D_0} + C_{52})\boldsymbol{s} + \\ (C_{61}\cdot \boldsymbol{D_0} + C_{62}) \end{bmatrix}$$

The values of the A_{ij}, B_{ij} and C_{ik} (i =1,2,3,4,5,6; j= 1,2,3; k=1,2) coefficients are reported in Table 2, where

A_{11}, B_{11} are measured in [mm^{-2}];

A_{12}, A_{21}, B_{12}, B_{21}, C_{11} are measured in [mm^{-1}];

A_{13}, A_{22}, A_{31}, B_{13}, B_{21}, B_{22}, B_{31}, C_{12}, C_{21} are dimensionless;

A_{23}, A_{32}, B_{23}, B_{32}, C_{22}, C_{31} are measured in [mm];

A_{33}, B_{33}, C_{32} are measured in [mm^2];

A_{41}, B_{41} are measured in [Nmm^{-4}];

A_{42}, A_{51}, B_{42}, B_{51}, C_{41} are measured in [Nmm^{-3}];

A_{43}, A_{52}, A_{61}, B_{43}, B_{52}, B_{61}, C_{42}, C_{51} are measured in [Nmm^{-2}];

A_{53}, A_{62}, B_{53}, B_{62}, C_{52}, C_{61} are measured in [Nmm^{-1}];

A_{63}, B_{63}, C_{62} are measured in [N].

Table 2 Values of the coefficients of the "Force-Pressure-Contraction" formula

A_{11}	A_{12}	A_{13}	B_{11}	B_{12}	B_{13}	C_{11}	C_{12}
-12.079	1122.2	-26214	0.882	-89.553	2331.4	-0.0366	-7.9276
A_{21}	A_{22}	A_{23}	B_{21}	B_{22}	B_{23}	C_{21}	C_{22}
43.917	-4364.9	100482	-1.9985	309.05	-7824.9	-4.9662	78.727
A_{31}	A_{32}	A_{33}	B_{31}	B_{32}	B_{33}	C_{31}	C_{32}
14.061	1969	-64578	-23.591	-1.3836	4592.1	345.94	-6378.4
A_{41}	A_{42}	A_{43}	B_{41}	B_{42}	B_{43}	C_{41}	C_{42}
2.5976	-247.07	5929.1	-0.1886	19.928	-534.44	0.0477	-2.2277
A_{51}	A_{52}	A_{53}	B_{51}	B_{52}	B_{53}	C_{51}	C_{52}
-9.1771	935.22	-21081	0.414	-66.297	1433.3	-0.2709	8.9142
A_{61}	A_{62}	A_{63}	B_{61}	B_{62}	B_{63}	C_{61}	C_{62}
3.888	-495.47	13380	0.6582	-22.524	-89.23	0.3005	-10.664

4. RESULTS AND DISCUSSION

The first part of the validation of the achieved formula was carried out by the comparison of the Force-Contraction curves obtained by the formula with those obtained by the numerical models. A first comparison was carried out with the curves from which the formula was derived; then, a comparison was carried out with curves referred to a model with D_0=35 mm, inside the convenient range of diameters adopted for the proposed method. Figure 12 shows the comparison of the analytical and numerical curves.

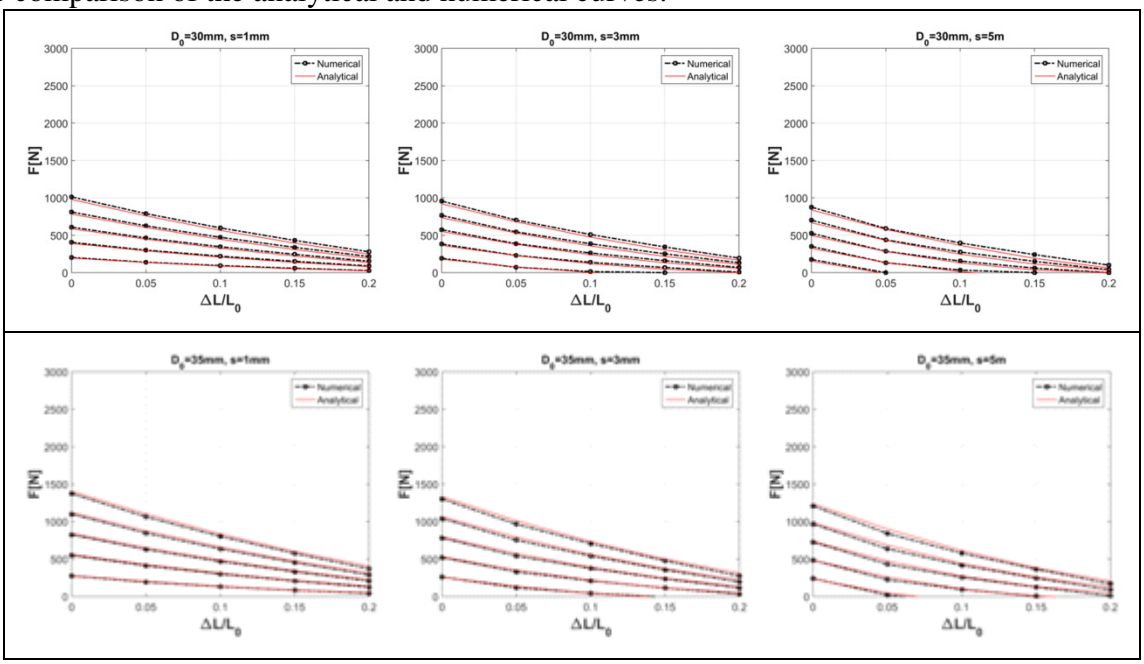

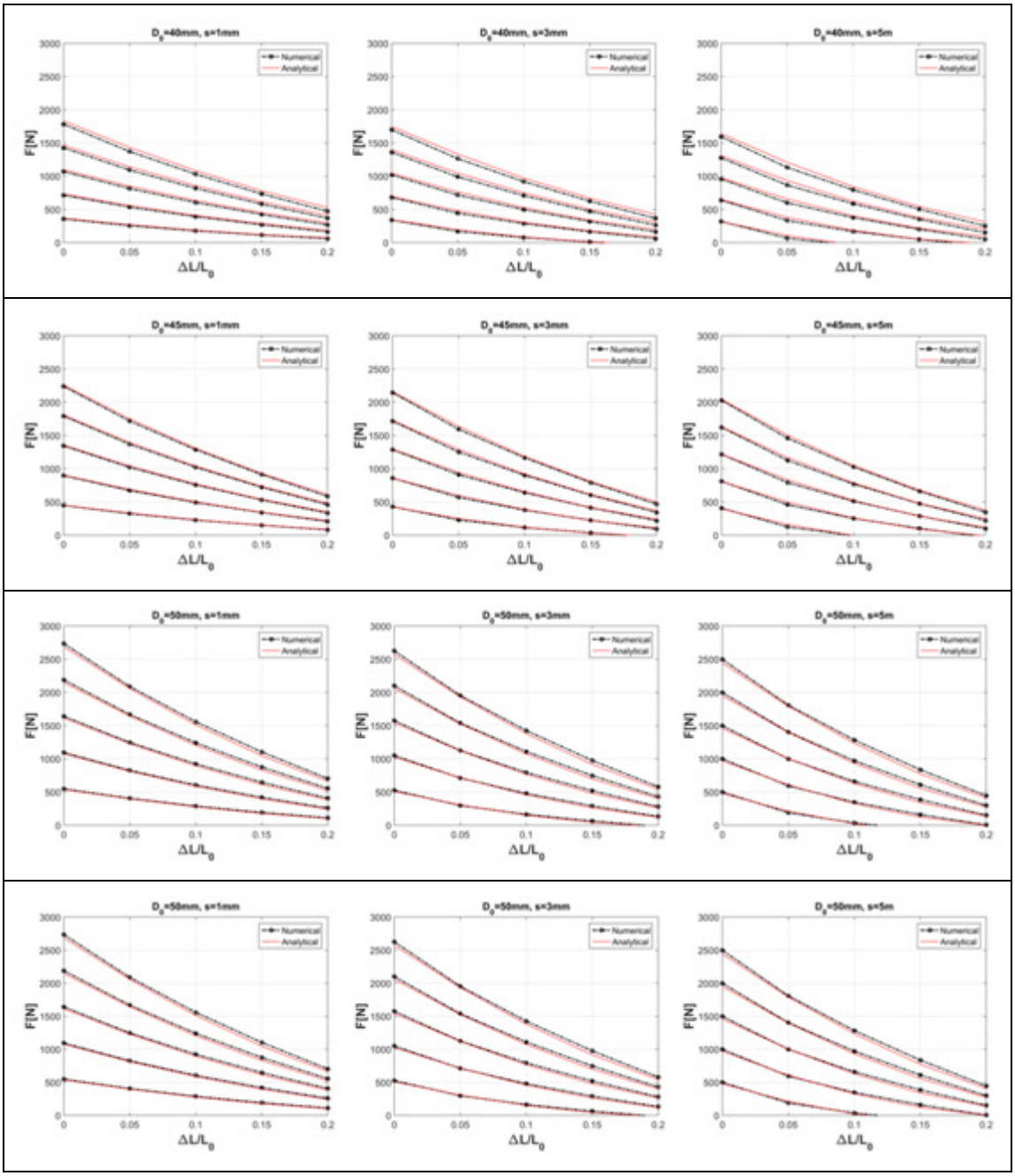

Figure 12 Analytical vs. numerical Force-Contraction curves

It can be noticed a good correspondence between the analytical and numerical curves. The maximum error is about 2% computed as:

$$\text{err} = \frac{\left|\text{F}_{i-analytical}(\bar{P}) - F_{i-numerical}(\bar{P})\right|}{\max\left(F_{i-numerical}(\bar{P})\right)} \quad (12)$$

The maximum force difference was equal to 50 N at the pressure of 0.25 MPa.

The second part of the validation of the achieved formula was carried out by the comparison of the isometric curves obtained by the analytical formula with those ones obtained by the above mentioned experimental model. The developed force was calculated and measured at five contraction ratios: 0%, 0.05%, 0.10%, 0.15% and 0.20 %.Results are shown in Figure 13.

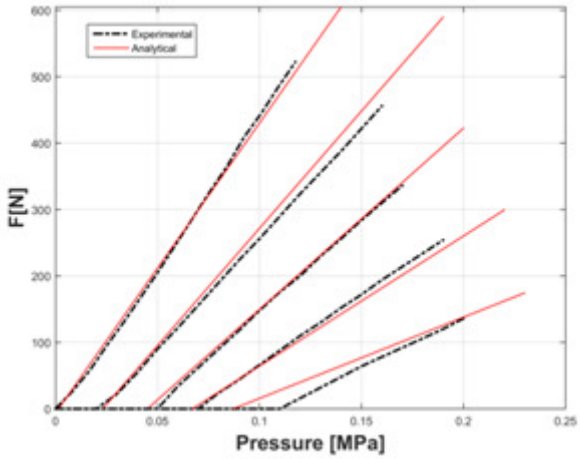

Figure 13 Analytical vs. experimental isometric curves

With the exception of the curve at the 0.20% contraction ratio, the analytical curves show a good fitting with the experimental ones. These results suggest that the formula can replace the use of the FE model in the range 30-50 mm of the diameters and in the range 1-5 mm of the thicknesses. In the final application, given a wanted force at a given contraction ratio, the formula can easily provide for a set of Force-Contraction curves: the proper MKM, depending on the thickness, the external diameter and the available pressure, is that one that satisfies the specifications.

5. CONCLUSIONS

Several models to predict the behaviour of MKMs exist in scientific literature. Nevertheless, the practical application of these models is limited because of their complexity, some parameters are difficult to be measured or evaluated and some formulations are only valid in particular ranges of geometrical parameters. Moreover, a formulation that takes into account all the typical parameters of MKMs does not exist. The present article proposes an analytical formula, based onthe external diameter at rest, the thickness, the pressure and the contraction ratio, to predict the developed force of MKMs whose material of the inner tube is a silicone rubber. The formula was achieved by a numerical approach carried out with a validated non-linear finite element model of such muscles. A method was defined to achieve the characteristic coefficients and the dependence of the developed force on the aforementioned parameters. Formula was achieved and validated in a convenient range of diameter, 30-50 mm, of thickness, 1-5 mm, of pressure, 0-0.25 MPa, and of contraction ratio, 0.00-0.20%. The encouraging results of the validation process suggest that this formula can replace the implemented FE model and can be used as a tool to design McKibben muscles starting from specifications of several applications in the field of industrial automation and robotics.

ACKNOWLEDGMENTS

Authors thank Eng. Stefano Colaiuda for his support during the development of the present research.

REFERENCES

[1] Morecki, A. Polish artificial pneumatic muscles. 4th International Conference on Climbing and Walking Robot,Karlsruhe, Germany, 2001.

[2] Tomori, H. and Nakamura, T. Theoretical Comparison of McKibben-Type Artificial Muscle and Novel Straight-Fiber-Type Artificial Muscle. International Journal of Automation Technology,5(4), 2011, pp. 544-550.

[3] Durante, F., Antonelli, M.G., Beomonte Zobel.P. and Raparelli, T. Development of a Straight Fibres Pneumatic Muscle. International Journal of Automation Technology,12(3), 2018, pp. 413-423.

[4] Schulte, H.F. The characteristic of the McKibben artificial muscle. National Academy of Sciences, National Research Council (eds) The Application of External Power in Prosthetics and Orthotics (Publication 874, Appendix H). Washington, DC: National Academy of Sciences, National Research Council; 1962; 94–115.

[5] Caldwell, D.G., Razak, A., Goodwin, M.J. Braided pneumatic muscle actuators. Conference on Intelligent Autonomous Vehicles (IFAC), Southampton, England,1993 pp. 507–512.

[6] Chou, C.P. and Hannaford, B. Measurement and modelling of McKibben pneumatic artificial muscles. IEEE Transactions on Robotics and Automation, 12(1), 1996, pp. 90–102.

[7] Tondu, B. and Lopez, P. Modeling and control of McKibben artificial muscle robot actuators. IEEE Control Systems, 20(2), 2000, pp.15–38.

[8] Immega, G.B. ROMAC actuators for micro robots. Micro Robotics and Teleoperators Workshop, IEEE Robotics and Automation Council, Hyannis, MA, 1987.

[9] Baldwin, H.A. Realizable models of muscle function. First Rock Biomechanics Symposium,New York, NY, 1967 pp.139–148.

[10] Daerden, F. and Lefeber, D. The concept and design of pleated pneumatic artificial muscles. International Journal of Fluid Power,2(3), 2001, pp.41–50.

[11] Villegas, D., Van Damme, M., Vanderborght, B., Beyl, P. and Lefeber, D. Third-generation pleated pneumatic artificial muscle for robotic applications: development and comparison with McKibben muscle. Advanced Robotics,26(11-12), 2012, pp.1205–1227.

[12] Antonelli, M.G., Beomonte Zobel, P., Raimondi, P., Raparelli, T. and Costanzo, G. An innovative brace with pneumatic thrusts for scoliosis treatment. International Journal of Design & Nature and Ecodynamics, 5(4), 2010, pp.1-14.

[13] Raparelli, T., Beomonte Zobel, P., Durante, F., Antonelli, M.G., Raimondi, P. and Costanzo, G. First clinical investigation on a pneumatic lumbar unloading orthosis. IEEE/ICME International Conference on Complex Medical Engineering, CME 2007, art. No. 4381959, pp.1327-1330.

[14] Antonelli, M.G., Beomonte Zobel, P., Durante, F. and Gaj, F. Development and testing of a grasper for NOTES powered by variable stiffness pneumatic actuation. International Journal of Medical Robotics and Computer Assisted Surgery,13(3), 2017, e1796.

[15] Antonelli, M.G., Beomonte Zobel, P., Durante, F. and Raparelli, T. Development and Pre-Clinical Investigation of a Massage Device for the Low Back. International Journal of Mechanical Engineering and Technology, 9(2), 2018, pp.742-754.

[16] Belforte, G., Eula, G., Ivanonv, A. and Sirolli, S.Soft pneumatic actuators for rehabilitation. Actuators, 3, 2014, pp.84–106.

[17] Noritsugu, T., Takaiwa, M. and Sasaki, D. Development of a pneumatic rubber artificial muscle for human support applications. 9th Scandinavian international conference on fluid power,Linkoping, Sweden, 2005.

[18] Noritsugu, T. Wearable power assist robot driven with pneumatic rubber artificial muscles. 2009 International Conference on Networking, Sensing and Control,Okayama, Japan, 2009.

[19] Greer, J.D., Morimoto, T.K., Okamura, A.M. and Hawkes, E.W. Series pneumatic artificial muscles (sPAMs) and application to a soft continuum robot. IEEE International Conference on Robotics and Automation (ICRA),Singapore, 2017 pp.5503-5510.

[20] Kim, S., Laschi, C. and Trimmer B. Soft robotics: a bioinspired evolution in robotics. Trends in Biotechnology, 31(5), 2013, pp.287-294.

[21] Antonelli, M.G., D'Ambrogio, W. And Durante, F. Development of a pneumatic soft actuator as a hand finger for a collaborative robot. ACM International Conference Proceedings Series,February 2018 pp.67-71.

[22] Noritsugu, T., Tanaka, T. and Yamanaha, T. Application of rubber artificial muscle manipulator as a rehabilitation robot. 5th IEEE International Workshop on Robot and Human Communication,Tsukuba, Japan, 1996 pp.112-117.

[23] Meng, W., Liu, Q., Zhang, M., Qingsong, A. and Sheng Quan, X. Compliance Adaptation of An Intrinsecally Soft Ankle Rehabilitation Robot Driven by Pneumatic Muscles. IEEE International Conference on Advanced Intelligent Mechatronics (AIM), Munich, Germany, 2017, pp.82-87.

[24] Polygerinos, P., Wang, Z., Galloway, K.C., Woodab, R.J. and Walshab, C.J. Soft robotic glove for combined assistance and at-home rehabilitation. Robotics and Autonomous Systems, 73, 2015, pp.135-143.

[25] Raparelli, T., Beomonte Zobel, P., Durante, F. The Design of a 2-dof Robot for Functional Recovery Therapy driven by Pneumatic Muscles. 10th Int. Workshop on Robotics in Alpe-Adria- Danube Region (RAAD), Vienna, Austria,2001 paper RD-0782001.

[26] Belforte, G., Eula, G., Ivanov, A., Raparelli, T. and Sirolli, S. Presentation of textile pneumatic muscle prototypes applied in an upper limb active suit experimental model. The Journal of Textile Institute, 109(6), 2017, pp.757-766.

[27] Durante, F., Beomonte Zobel, P. and Raparelli, T. Development of an active orthosis for inferior limb with light structure.Mechanisms and Machine Science, 49, 2018, pp. 833-841.

[28] Durante, F., Antonelli, M.G. and Beomonte Zobel, P. Development of an active exoskeleton for assisting back movements in lifting weights. International Journal of Mechanical Engineering and Robotics Research, 7(4), 2018, pp.353-360.

[29] Sasaki, D., Noritsugu, T. and Takaiwa, M. Development of Active Support Splint Driven by Pneumatic Soft Actuator (ASSIST). Journal of Robotics and Mechatronics, 16(5), 2004, pp.497-503.

[30] Noritsugu, T., Sasaki, D., Kameda, M., Fukunaga, A. and Takaiwa, M.Wearable Power Assist Device for Standing Up Motion Using Pneumatic Rubber Artificial Muscles. Journal of Robotics and Mechatronics, 19(6), 2007, pp.619-628.

[31] Kobayashi, H., Takamitsu, A. and Hashimoto, T. Muscle Suit Development and Factory Application. International Journal of Automation Technology, 3(6), 2009, pp.709-715.

[32] Wu, M., Driver, T., Wu, S. andShen, X.Design and Preliminary Testing of a Pneumatic Muscle-Actuated Transfemoral Prosthesis. Journal of Medical Devices, 8(4), 2014, pp.044502-044502-7.

[33] Huang, S., Wensman, J.P. and Ferris, D.P. An Experimental Powered Lower Limb Prosthesis Using Proportional Myoelectric Control. Journal of Medical Devices, 8(2), 2014, pp.024501-024501-5.

[34] Koceska, N., Koceski, S., Durante, F., Beomonte Zobel, P. and Raparelli, T. Control architecture of a 10 DOF lower limbs exoskeleton for gait rehabilitation. International Journal of Advanced Robotic Systems, 10, 2013, art. no. 68.

[35] Raparelli, T., Beomonte Zobel, P. and Durante F. Mechanical Design of a 3-dof parallel robot actuated by smart wires. Proceedings of EUCOMES 2008, The 2nd European Conference on Mechanism Science, 2009 pp.271-278.

[36] Raparelli, T., Beomonte Zobel, P. and Durante, F. A robot actuated by shape memory alloy wires. IEEE International Symposium on Industrial Electronics, (2), 2002, art. no. 1026323, pp.420-423.

[37] Antonelli, M.G., Auriti, L. Beomonte Zobel, P. and Raparelli, T. Development of a new harvesting module for saffron flower detachment. Romanian Review Precision Mechanics, Optics and Mechatronics, 39, 2011, pp.163-168.

[38] Koceski, S., Koceska, N., Beomonte Zobel, P. and Durante, F. Characterization and modelling of a 3D scanner for mobile robot navigation, 17th Mediterranean Conference on Control and Automation, MED 2009, 2009 art.no. 5164518 pp.79-84.

[39] Klute, G.K. and Hannaford, B. Accounting for Elastic Energy Storage in McKibben Artificial Muscle Actuators. Journal of Dynamic Systems, Measurement and Control, 122(2), 2000, pp.386-388.

[40] Tsagarakis, N., Caldwell, D.G. Improved modelling and assessment of pneumatic muscle actuators. International conference on robotics and automation,San Francisco, CA,2000 pp.3641–3646.

[41] Davis, S. and Caldwell, D.G. Braid effect on contractile range and friction modeling in pneumatic muscle actuators. The International Journal of Robotics Research, 25(4), 2006, pp.359–369.

[42] Sorge, F. and Cammalleri, M. A theoretical approach to pneumatic muscle mechanics. IEEE/ASME international conference on advanced intelligent mechatronics,Wollongong, NSW, Australia,2013 pp.1021–1026.

[43] Chen, D.H. and Ushijima K. Prediction of the mechanical performance of McKibben artificial muscle actuator. International Journal of Mechanical Sciences, 78, 2014, pp.183-192.

[44] Belforte, G., Raparelli, T. and Sirolli, S.A Novel Geometric Formula for Predicting Contractile Force in McKibben Pneumatic Muscles. International Journal of Automation Technology, 11(3), 2017, pp.368-377.

[45] Antonelli, M.G., Beomonte Zobel, P., Durante, F. and Raparelli, T.Numerical modelling and experimental validation of a McKibben pneumatic muscle actuator. Journal of Intelligent Material Systems and Structures, 28(19), 2017, pp.2737-2748.

[46] Daerden, F. and Lefeber, D. Pneumatic artificial muscles: actuators for robotics and automation. European Journal of Mechanical and Environmental Engineering, 47(1), 2002, pp.11–21.

[47] Wakimoto, S., Suzumori, K. and Takeda, J. Flexible artificial muscle by bundle of McKibben fiber actuators. IEEE/ASME international conference on advanced intelligent mechatronics,Budapest, Hungary,2011 pp.457–462.

[48] Iwata, K., Suzumori, K. and Wakimoto, S. A method of designing and fabricating McKibben muscles driven by 7 MPa hydraulics. International Journal of Automation Technology, 6(4), 2012, pp.482–487.

[49] Nozaki, T. and Noritsugu, T. Motion analysis of McKibben type pneumatic rubber artificial muscle with finite element method. International Journal of Automation Technology, 8(2), 2014, pp.147–158.